



Synthesis and characterization of chitosan–polyvinylpyrrolidone–bovine serum albumin-coated magnetic iron oxide nanoparticles as potential carrier for delivery of tamoxifen

G. Prabha¹ · V. Raj²

Received: 26 May 2017 / Accepted: 28 December 2017 / Published online: 15 January 2018
© Iranian Chemical Society 2018

Abstract

The proposed study examined the preparation of chitosan (CS)–polyvinylpyrrolidone (PVP)–bovine serum albumin (BSA)-coated magnetic iron oxide (Fe_3O_4) nanoparticles (Fe_3O_4 –CS–PVP–BSA) to use as potential drug delivery carriers for delivery of tamoxifen drug (TAM). The anticancer drug selected in this study was tamoxifen which can be used for the human breast cancer treatment. These prepared nanoparticles were characterized by FTIR, XRD, SEM, AFM, TEM, CD and VSM techniques. The swelling studies have been measured at different (10, 20, 30, 40, 50%) drug loading. The mean particle size of the tamoxifen-loaded nanoparticles system (Fe_3O_4 –CS–TAM, Fe_3O_4 –CS–TAM–PVP and Fe_3O_4 –CS–TAM–PVP–BSA) as measured by Malvern Zetasizer ranged between 350 ± 2.3 and 601 ± 1.7 nm. As well as these drug-loaded nanoparticles were positively charged. The zeta potential was in the range of 28.9 ± 3.5 and 50.8 ± 3.9 mV. The encapsulation efficiency was between 63.60 ± 2.11 and $96.45 \pm 2.12\%$. Furthermore, in vitro release and drug loading efficiency from the nanoparticles were investigated. The cytotoxicity of prepared nanoparticles was verified by MTT assay. In vitro release studies were executed in 4.0 and 7.4 pH media to simulate the intestinal and gastric conditions and different temperature (37 and 42 °C). Hence, the prepared tamoxifen-loaded nanoparticles system (Fe_3O_4 –CS–TAM, Fe_3O_4 –CS–TAM–PVP and Fe_3O_4 –CS–TAM–PVP–BSA) could be a promising candidate in cancer therapy.

Keywords Chitosan · Polyvinylpyrrolidone · Bovine serum albumin · Tamoxifen · Drug delivery · In vitro release

Introduction

Magnetic iron oxide nanoparticles are developing as favorable contenders for applications in biomedical investigation including drug delivery [1], hyperthermia [2], magnetic resonance imaging [3], tumor progression [4], cell mechanics [5], in vivo tracking of stem cells, cell separation and nucleic acid [6, 7], owing to their biocompatibility, superparamagnetic property and ultrafine sizes [8]. Nevertheless, the SPION inclined to become big aggregates due to the strong magnetic dipole–dipole

attractions amid particles [9, 10]. The surface of SPIONs is modified with various surfactants to increase their stability and biocompatibility [11], oxide [12] or polymeric compounds [13, 14]. Currently, though both natural and synthesized macromolecules have been effectively used to stabilize SPIONs, a number of natural polymers, for example, pullulan [15], dextran [16], starch [17], and bovine serum albumin (BSA) [18], which could give biocompatibility, biodegradability, hydrophilic properties, and good solubility, were employed as defensive layers on the surface of SPIONs. Biocompatible synthetic polymers are being used as a substitute to the natural polymers. Effortlessly controlled structures, for example, molecular weight, molecular-weight distribution and chemical structure, tailor-built surfaces, and functional groups on the nanoparticles are the benefits of synthetic polymers that are utilized as stabilizers for magnetic iron oxide nanoparticles [19, 20].

Chitosan is a linear cationic polysaccharide formed by deacetylation of chitin naturally extracted from shells

✉ G. Prabha
gprabhagovinn@gmail.com

¹ Department of Chemistry, Indian Institute of Technology Madras, Chennai, Tamil Nadu, India

² Advanced Materials Research Laboratory, Department of Chemistry, Periyar University, Salem, Tamil Nadu, India

of shrimps and crabs, or isolated from the cell walls of fungi. This linear cationic polysaccharide is made out of randomly distributed β (1 \rightarrow 4) linked d-glucosamine and *N*-acetyl-d-glucosamine units. This cationic polysaccharide has garnered increasing consideration in biomedical applications, due to its plentiful accessibility, distinctive muco-adhesiveness, intrinsic pharmacological and useful biological properties, for example, low toxicity, excellent biodegradability, good biocompatibility and non-immunogenicity and also a high positive charge that effortlessly forms polyelectrolyte complexes with negatively charged units [21].

Polyvinylpyrrolidone (PVP) molecules consist of pyrrolidone functional groups which could effortlessly halt crystals of Fe_3O_4 nanoparticles that can help to form ultra-small magnetic particles and halt the aggregation of the nanoparticles. It is a renowned macromolecule surfactant with many advantages such as high surface activity, biocompatibility, strong adsorption ability and non-toxicity. It has been well technologically developed for the synthesis of SPIONs, due to its good biocompatibility and aqueous dispersing ability [22, 23].

Bovine serum albumin (BSA) is a naturally existing biomaterial that has been used as a matrix in nanoparticle preparations. Because of its proteinous nature, this protein is also biodegradable, biocompatible, non-immunogenic, and non-toxic [24, 25]. The albumin nanoparticles are a good system for antigen and drug delivery [26, 27].

Tamoxifen (TAM), a nonsteroidal anti-estrogen compound and strong hydrophobic drug, is most commonly used in controlling breast cancer and high danger patients [28]. While tamoxifen was mainly utilized as a drug against hormone-dependent breast cancers [29], it has, likewise, been utilized as a part of the treatment of hormone-insensitive estrogen receptor-negative breast cancers [30]. Tamoxifen prevents cell proliferation and persuades apoptosis in breast cancer cells [31]. After long-term therapy, tamoxifen has some major side effects such as endometrial cancer and advancement of drug resistance that may lead to further progression of the tumor [32]. These undesirable side effects of tamoxifen as well as numerous barriers to the effective administration of drugs demands for targeted delivery to the site of tumor and better uptake by the tumor cells.

To conquer the unwanted side effects of tamoxifen and to increase the concentration at the tumor site, tamoxifen could be entrapped in colloidal drug carriers. Different types of polymeric nanoparticles have been employed for the delivery of tamoxifen, which include poly(isohexylcyanoacrylate) [33], poly(lactic-co-glycolic acid) [34], poly(butylcyanoacrylate) [35], chitosan [36], liposomes [37] and gelatin [38]. In addition, Dries et al. [39] employed human serum albumin (HSA) which may offer an improved means of delivery in terms of

improved uptake by the tumor and increased local concentration of the drug at the receptor site.

This work is focused on the preparation of the tamoxifen-loaded nanoparticles (Fe_3O_4 -CS-TAM, Fe_3O_4 -CS-TAM-PVP and Fe_3O_4 -CS-TAM-PVP-BSA) which were characterized in a detailed manner. Besides the drug encapsulation efficiency, loading capacity, drug release properties and cytotoxicity of the prepared nanoparticles were also studied.

Materials and methods

Materials

Iron (II) chloride tetrahydrate ($\text{FeCl}_2 \cdot 4\text{H}_2\text{O}$), Iron (III) chloride hexahydrate ($\text{FeCl}_3 \cdot 6\text{H}_2\text{O}$), chitosan (MW = 60–90 kDa; degree of *N*-deacetylation 75–80%), polyvinylpyrrolidone (PVP, MW: 10,000), bovine serum albumin (BSA, purity 96–99%), sodium tripolyphosphate (TPP), ammonium hydroxide (25 wt%), phosphate-buffered saline (PBS), Tamoxifen, dimethyl sulfoxide (DMSO) and 3-(4,5-dimethylthiazole-2-yl)-2,5-diphenyl tetrazolium bromide (MTT) were obtained from Sigma–Aldrich (St. Louis, MO, USA). MCF-7 and VERO cell lines were bought from National Center for Cell Sciences (NCCS), Pune, India. All chemicals were utilized without further treatment.

Preparation of superparamagnetic Fe_3O_4 nanoparticles (SPIONs)

Magnetic iron oxide nanoparticles (Fe_3O_4) were prepared by using the coprecipitation way as reported in our recent publication [40]. Briefly, iron (II) chloride tetrahydrate (0.6 g) and iron (III) chloride hexahydrate (0.82 g) were liquefied in 10 mL of double distilled water in three-necked bottle. The mixture was magnetically stirred at 30 °C for 20 min to attain a homogeneous solution. Consequently, 2.5 mL of ammonium hydroxide (NH_4OH) (28%) solution was added dropwise into the homogeneous solution to maintain the pH level at 11. The stirring was continued for 40 min, and then, the mixture was heated to 80 °C for 45 min with constant fast stirring. The solution appears in black color, which is the required condition for precipitation of the contained particles. Finally, the precipitate of Fe_3O_4 nanoparticles was filtered, washed many times with distilled water and ethanol. Lastly, the Fe_3O_4 particles were then dried in a vacuum oven at 50 °C for 24 h to confirm the complete removal of water.

Preparation of superparamagnetic (Fe_3O_4 -CS-TAM) nanoparticles

The beforehand reported technique was followed in the preparation of CS nanoparticles [41]. In brief, 5 mg/mL

of Fe_3O_4 and 4 mg/mL of CS were initially dissolved in a 1% acetic acid solution and the resultant suspension was subjected to sonication for 30 min to acquire a homogeneous Fe_3O_4 -CS solution, and tamoxifen (4–20 mg) was dissolved alone in dehydrated alcohol (ultrasonicated for 20 min) and prepared at various concentrations (10–50%, using 4–20 mg of tamoxifen, respectively). At this point, the various concentrations of the tamoxifen solution was added to 10 mL of the Fe_3O_4 -CS solution under magnetic stirring (1000 rpm) at 30 °C to attain Fe_3O_4 -CS-TAM solution. The Fe_3O_4 -CS-TAM solution was added dropwise (utilizing a dispensable syringe) into 4 mL of the sodium tripolyphosphate (TPP) solution (2 mg/mL) under magnetic stirring (~ 200 rpm) at 30 °C. The Fe_3O_4 -CS-TAM nanoparticles were produced rapidly. The magnetic Fe_3O_4 -CS-TAM nanoparticle suspension was stirred at 27 °C for 90 min for more cross-linking of the nanoparticles. At last, the Fe_3O_4 -CS-TAM nanoparticles were gathered by centrifugation at 1500 rpm and dried in vacuum oven at 50 °C for 24 h.

Preparation of the Fe_3O_4 -CS-TAM-PVP and Fe_3O_4 -CS-TAM-PVP-BSA nanoparticles

The different percentage of encapsulated Fe_3O_4 -CS-TAM nanoparticles in the PVP and BSA solution were prepared by a procedure depicted in our past study [42]. Initially, 10% of PVP solution was prepared in distilled water. The solution was progressively added to the various percentage of encapsulated Fe_3O_4 -CS-TAM nanoparticles under constant magnetic stirring at 30 °C for 1 h. The resulting various percentages of encapsulated nanocomposites (Fe_3O_4 -CS-TAM-PVP) were gathered by centrifugation at 1500 rpm and freeze-dried at – 40 °C for 24 h. Likewise, 20% of BSA solution was prepared in distilled water and progressively added to the various percentages of the encapsulated Fe_3O_4 -CS-TAM-PVP nanocomposites under constant magnetic stirring at 30 °C for 1 h. Finally, the resulting various percentages of the encapsulated nanocomposites (Fe_3O_4 -CS-TAM-PVP-BSA) were gathered by centrifugation at 1500 rpm and freeze-dried at – 40 °C for 24 h.

Characterization techniques

The zeta potential and particle size of the newly prepared drug-loaded (Fe_3O_4 -CS-TAM, Fe_3O_4 -CS-TAM-PVP and Fe_3O_4 -CS-TAM-PVP-BSA) nanocomposites were determined by using Zetasizer (Malvern Instruments, UK). FTIR (FTIR; Perkin-Elmer Spectrum RX100) in the range of 400–4000 cm^{-1} was used to identify the functional groups in the prepared nanocomposites. X'pert pro PANalytical Instrument using $\text{Cu K}\alpha_1$ radiation ($\lambda = 1.5418 \text{ \AA}$) and scan range of 2θ between 1° and 80° at 295 K was used

to studied the crystallinity of pure Fe_3O_4 nanoparticles and Fe_3O_4 -CS, Fe_3O_4 -CS-PVP and Fe_3O_4 -CS-PVP-BSA nanocomposites. The surface morphology of prepared nanocomposites was examined by scanning electron microscope (Hitachi, Japan, S-3400N). The average size and surface topography of the prepared nanoparticles (Fe_3O_4 -CS-TAM, Fe_3O_4 -CS-TAM-PVP and Fe_3O_4 -CS-TAM-PVP-BSA) were examined by atomic force microscopy (AFM), and the all images were examined using a multimode scanning probe microscope (NTMDT, NTEGRA Prima, Russia) operating in the contact mode (antimony and doped Si probe). The developed nanoparticles were dispersed in methanol solvent followed by bath sonication for 20 min. Further, they were spun-coated over plain glass plate to form a thin film which was used for AFM analysis. The scan area was $20 \times 20 \mu\text{m}$. The surface morphology of the raw Fe_3O_4 nanoparticle and drug-loaded Fe_3O_4 -CS, Fe_3O_4 -CS-PVP and Fe_3O_4 -CS-PVP-BSA nanoparticles system was examined by transmission electron microscopy (TEM, Hitachi H-600-II). The nanoparticles for the TEM analysis were prepared by drying the dispersion on amorphous carbon-coated copper grids. Far-UV CD measurements were recorded on a JASCO J-720 spectropolarimeter with a 0.1 cm path length of cylindrical quartz cell at 25 °C, with a fixed BSA concentration of 4 μM . The CD spectra were recorded from 190 to 270 nm, and each spectrum was an average of three scans at a rate of 10 nm min^{-1} . Each sample was prepared starting from the stock solutions to the final 4 μM BSA and the concentration of Fe_3O_4 -CS-TAM-PVP-BSA ranging from 0–72 μM in 10 mM PBS. Data were fitted by using the software described in <http://cbdm-01.zdv.uni-mainz.de/~andrade/k2d3/>. The magnetic possessions of CS, PVP and BSA-coated Fe_3O_4 nanoparticles and uncoated Fe_3O_4 nanoparticles were investigated using Vibrating Sample Magnetometer (VSM) (Lake Shore Company, OH).

Evaluation of encapsulation efficiency (EE) and loading capacity (LC)

Drug loading capacity and encapsulation efficiency of TAM-loaded nanoparticles (Fe_3O_4 -CS-TAM, Fe_3O_4 -CS-TAM-PVP and Fe_3O_4 -CS-TAM-PVP-BSA) were evaluated after separation of nanoparticles from the aqueous nanoparticle suspension by ultra-centrifugation at 11,000 rpm at 23 °C for 40 min. The centrifuged nanoparticles were lyophilized, weighed and noted. The quantity of free TAM in the supernatant was observed by using UV-Visible spectrophotometer at the wavelength of 254 nm. The percentage of EE and LC of TAM-loaded nanoparticles (Fe_3O_4 -CS-TAM, Fe_3O_4 -CS-TAM-PVP and Fe_3O_4 -CS-TAM-PVP-BSA) were calculated by using the

subsequent Eqs. 1 and 2 [43]. The method was performed in triplicate.

$$EE = (\text{Total amount of TAM} - \text{amount of free TAM in the supernatant}) / \text{Total amount of TAM} \times 100 \quad (1)$$

$$LC = (\text{Total amount of TAM} - \text{amount of free TAM in the supernatant}) / \text{weight of nanoparticles} \times 100 \quad (2)$$

Swelling studies

Nanoparticles (0.1 g) were permitted to swell in a fixed volume of phosphate-buffered saline (PBS) pH 4.0 for a predetermined time period, and subsequently, the nanoparticles were taken out from the PBS and slowly pressed in-between the two filter papers to eliminate excess of PBS and finally weighed. A time period of 24 h was found to be sufficient for equilibrium swelling. The swelling percentage was determined by the following formula [44].

$$\text{Swelling (\%)} = [(w_2 - w_1) / w_1] \times 100$$

where W_1 is the denote the initial weight of nanoparticles before swelling, and W_2 is the final weight of nanoparticles after swelling for a predetermined time. All the experiments were done in triplicates.

Evaluation of in vitro drug release

In vitro TAM release profiles from TAM-loaded nanoparticles ($\text{Fe}_3\text{O}_4\text{-CS-TAM-PVP}$) were determined as follows. A known amount of TAM-loaded nanoparticles (0.1 mg) was suspended in a 10 mL of PBS (phosphate-buffered saline) at two different pH (4.0 and 7.4) and temperature (37 and 42 °C), respectively. The resultant suspension was stirred at 150 rpm and the temperature was kept up at 37 and 42 °C for a correct time intervals and 5 mL aliquots of the dissolution medium were withdrawn at suitable time intervals and suddenly equal volume of fresh PBS was supplemented to maintain the constant volume. The amount of TAM released was measured by UV-Visible spectrophotometer at a wavelength of 254 nm. All tests were performed in triplicate in order to minimize the variational mistake. The release profiles were plotted as the relative percentages of TAM against time.

Cell culture

For cell culture tests VERO and MCF-7 cell lines were used. MCF-7 and VERO cell lines were preserved in Minimum Essential Medium (MEM) supplemented with 10%

heat-inactivated Fetal Bovine Serum (FBS) and 100 units/mL Penicillin/ Streptomycin. The cells were later incubated

under standard cell culture conditions at 37 °C in 5% carbon dioxide (CO_2) atmosphere. After incubating for a required period of time, the cells were washed off the culture flask using trypsin-EDTA. The cell suspension was centrifuged at 1500 rpm for 3 min and afterward resuspended in complete media, counted and used for further cell culture studies.

Cytotoxicity studies

The cytotoxicity of free TAM, TAM-loaded nanocomposites ($\text{Fe}_3\text{O}_4\text{-CS-TAM}$, $\text{Fe}_3\text{O}_4\text{-CS-TAM-PVP}$ and $\text{Fe}_3\text{O}_4\text{-CS-TAM-PVP-BSA}$) and unloaded nanocomposites ($\text{Fe}_3\text{O}_4\text{-CS-PVP-BSA}$) were carried out on VERO and MCF-7 cell lines by using the 3-(4,5-dimethylthiazole-2-yl)-2,5-diphenyl tetrazolium bromide (MTT) assay. VERO and MCF-7 cells were seeded on a 96-well plates with a density of 1×10^4 cells/well and allowed to attach for 1 day. Then, different concentrations of the free TAM, TAM-loaded nanocomposites ($\text{Fe}_3\text{O}_4\text{-CS-TAM}$, $\text{Fe}_3\text{O}_4\text{-CS-TAM-PVP}$ and $\text{Fe}_3\text{O}_4\text{-CS-TAM-PVP-BSA}$) and unloaded nanocomposites ($\text{Fe}_3\text{O}_4\text{-CS-PVP-BSA}$) were added into the well and incubated for 48 h. At that point, MTT solution was added to every well and the plates were incubated for another 4 h at 37 °C. After being washed for three times with PBS buffer, 150 μL of DMSO was added to every well to dissolve the formazan crystals. The absorbance of the solutions was then measured at 570 nm (UVM 340 Microplate Spectrophotometer, Biochrom Asys). The cell viability (%) was related to the control wells containing untreated cells with new cell culture medium and was calculated by the following equation:

$$\text{Cell viability (\%)} = (\text{absorption test} / \text{absorption control}) \times 100.$$

Statistical analysis

SPSS 18 program was used to analyze the data. All data were assessed by one-way ANOVA. Values of $P < 0.05$ were considered as statistically significant.

Table 1 The particle size of Fe₃O₄-CS-TAM, Fe₃O₄-CS-TAM-PVP and Fe₃O₄-CS-TAM-PVP-BSA nanocomposites

Concentration of TAM (%)	Particle size (nm) mean \pm SD		
	Fe ₃ O ₄ -CS-TAM	Fe ₃ O ₄ -CS-TAM-PVP	Fe ₃ O ₄ -CS-TAM-PVP-BSA
10	350 \pm 2.3	440 \pm 2.0	545 \pm 1.2
20	362 \pm 2.7	456 \pm 3.2	570 \pm 1.9
30	378 \pm 2.7	479 \pm 4.8	582 \pm 1.4
40	400 \pm 2.1	510 \pm 2.9	595 \pm 1.0
50	420 \pm 2.6	525 \pm 2.3	601 \pm 1.7

Table 2 The zeta potential values of Fe₃O₄-CS-TAM, Fe₃O₄-CS-TAM-PVP and Fe₃O₄-CS-TAM-PVP-BSA nanocomposites

Concentration of TAM (%)	Zeta potential (mV) mean SD		
	Fe ₃ O ₄ -CS-TAM	Fe ₃ O ₄ -CS-TAM-PVP	Fe ₃ O ₄ -CS-TAM-PVP-BSA
10	28.9 \pm 3.5	30.1 \pm 5.2	36.1 \pm 4.2
20	32.7 \pm 9.1	34.7 \pm 3.2	39.7 \pm 3.1
30	35.5 \pm 7.2	37.9 \pm 7.0	42.7 \pm 6.9
40	38.6 \pm 7.6	43.2 \pm 5.2	48.3 \pm 7.1
50	44.8 \pm 6.3	46.0 \pm 2.4	50.8 \pm 3.9

TAM tamoxifen, Fe₃O₄ magnetic iron oxide nanoparticles, CS chitosan, PVP polyvinylpyrrolidone, BSA bovine serum albumin, SD standard deviation for three determinations

n = 3. The experiments were repeated twice

Results and discussion

Characterization of prepared nanoparticles

Particle size and zeta potential

The particle size and zeta potential of the TAM drug-loaded nanocomposites (Fe₃O₄-CS-TAM, Fe₃O₄-CS-TAM-PVP and Fe₃O₄-CS-TAM-PVP-BSA) systems are presented in Tables 1 and 2. Particle size of nanoparticles plays a significant role in clearance of reticuloendothelial cells. The particle size of the (10%) TAM drug-loaded (Fe₃O₄-CS-TAM, Fe₃O₄-CS-TAM-PVP and Fe₃O₄-CS-TAM-PVP-BSA) nanocomposites systems are observed to be 350 \pm 2.3, 440 \pm 2.0 and 545 \pm 1.2 nm, respectively, as appeared in Table 1. The raise in size might be ascribed to the loading of TAM on the nanocarrier (Fe₃O₄-CS, Fe₃O₄-CS-PVP and Fe₃O₄-CS-PVP-BSA) particles. Increase in the percentage of TAM encapsulation caused a minor raise in the size of the nanoparticles. The addition of PVP and BSA to Fe₃O₄-CS-TAM once

again increased the size of the nanoparticles. Zeta potential briefs about the charge on the surface of the nanoparticles and acting a significant role in the stability of the particles in suspension through the electrostatic repulsion among the nanoparticles [45]. Profoundly charged colloidal systems, whether positively or negatively charged, indicate little aggregation inclinations for the reason that of electrical repulsion. The zeta potential values for the prepared (10%) TAM drug-loaded (Fe₃O₄-CS-TAM, Fe₃O₄-CS-TAM-PVP and Fe₃O₄-CS-TAM-PVP-BSA) nanocomposites systems are observed to be 28.9 \pm 3.5, 30.1 \pm 5.2, 36.1 \pm 4.2, respectively, as shown in Table 2. Everyone these values lie in that stable range, demonstrating that the prepared nanoparticles systems are stable. The positive surface charge of TAM-loaded nanocomposites (Fe₃O₄-CS-TAM, Fe₃O₄-CS-TAM-PVP and Fe₃O₄-CS-TAM-PVP-BSA) can be credited to the presence of the residual protonated amino groups of CS molecules trapped onto the surface of the nanoparticles [46, 47]. This positive charge is alluring so as to avoid particles aggregation and to stimulate electrostatic interaction with the overall negative charge of the cell membrane [48]. Therefore, positively charged nanoparticles are perfect option for the preparation of drug delivery systems in the therapy of cancer-related diseases.

Fourier transmission infrared spectroscopy (FTIR) analysis

Figure 1 demonstrates the FTIR spectra of different samples [(A) Fe₃O₄ MNPs, (B) Fe₃O₄-CS, Fe₃O₄-CS-PVP and Fe₃O₄-CS-PVP-BSA nanocomposites loaded with 10% of TAM] respectively. From the spectrum of pure iron oxide in (Fig. 1a), we can see that the peaks at about 3349, 1634 and 586 cm⁻¹ are the characteristic absorption of O-H stretching, O-H bending and Fe-O stretching vibrations, respectively [49]. Yet, the characteristic peak of Fe-O is shifted to 577, 562 and 570 cm⁻¹ in the spectrum of Fe₃O₄-CS-TAM, Fe₃O₄-CS-TAM-PVP and Fe₃O₄-CS-TAM-PVP-BSA nanocomposites respectively. Compared with pure Fe₃O₄ nanoparticles (Fig. 1a), the spectrum of Fe₃O₄-CS-TAM has two characteristic peaks of CS at 1640 cm⁻¹ which indicates the characteristic of C=O stretching vibration (connected with NH₂) and the band at 1067 cm⁻¹ is because of the glycosidic bond stretching vibrations respectively. The addition of PVP and BSA leads to the shifting of CO absorption bands from 1640 to 1667 cm⁻¹. The outcomes indicate that the Fe₃O₄-CS is coordinated via CO group in PVP and prove the strong electrostatic interaction between PVP and CS. In addition, the absorption band at 1667 cm⁻¹ appeared in the spectrum of Fe₃O₄-CS-TAM-PVP-BSA is assigned to the stretching vibrations of C=N bond and N-H bond in BSA molecules. Similarly, glycosidic bond is shifted from 1067 to 1098 cm⁻¹ due to the C-O-C stretching

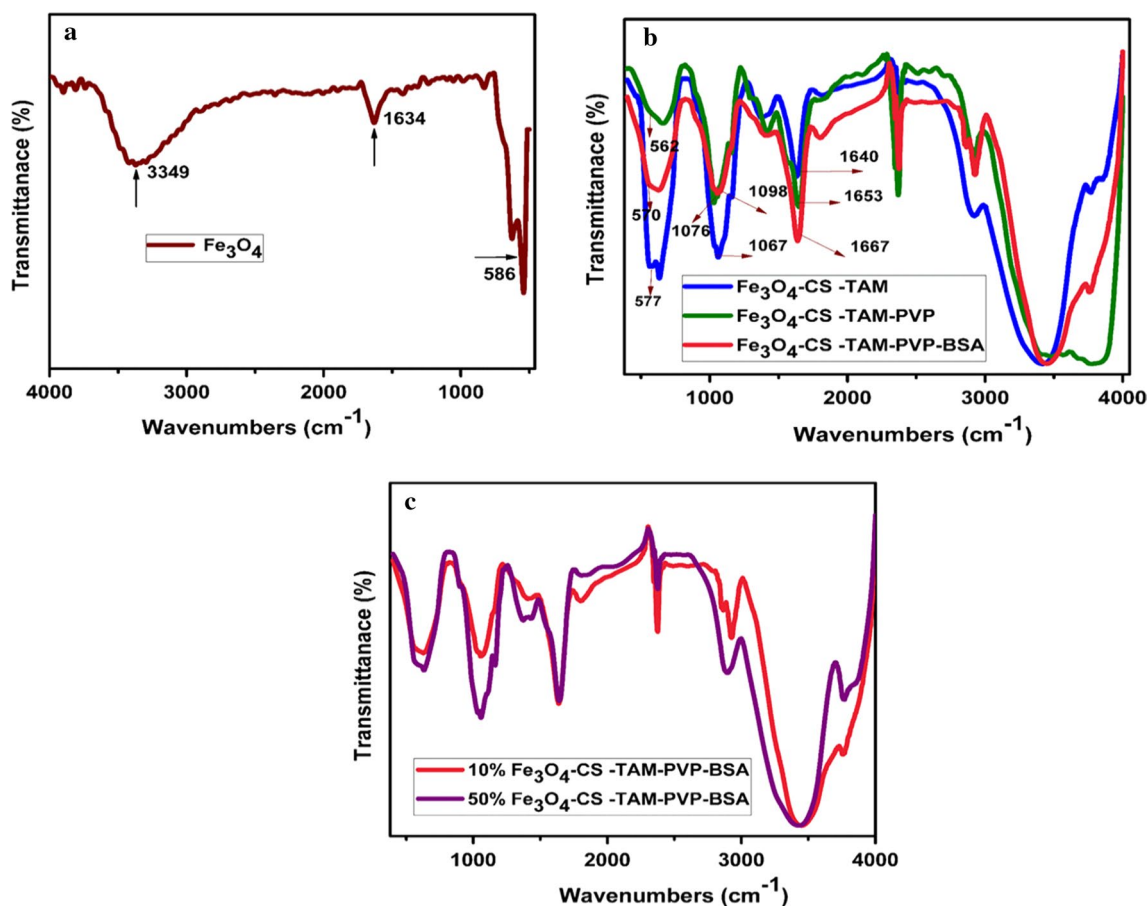


Fig. 1 a FTIR spectrum of pure Fe_3O_4 , b 10% of tamoxifen-loaded (Fe_3O_4 -CS-TAM, Fe_3O_4 -CS-TAM-PVP and Fe_3O_4 -CS-TAM-PVP-BSA) nanoparticles and c 10 and 50% of tamoxifen-loaded (Fe_3O_4 -CS-TAM-PVP-BSA) nanoparticles

vibration of PVP. Moreover, most of the intense characteristic peaks of TAM are not noticed at the same position in the drug-loaded nanocomposites, demonstrating a strong interaction between the drug and the polymer-coated magnetic nanocomposites. Figure 1c displays the FTIR spectra of the Fe_3O_4 -CS-PVP-BSA nanocomposites loaded with 10 and 50% of TAM. The spectra of the various concentration of TAM-loaded nanocomposites show the same peaks that fluctuated only in the intensity of the peaks.

X-ray diffraction (XRD) analysis

The XRD patterns of pure Fe_3O_4 and Fe_3O_4 -CS, Fe_3O_4 -CS-PVP and Fe_3O_4 -CS-PVP-BSA nanocomposites are displayed in Fig. 2. The pure Fe_3O_4 and Fe_3O_4 -CS, Fe_3O_4 -CS-PVP and Fe_3O_4 -CS-PVP-BSA nanocomposites display same characteristic diffraction peaks at $2\theta = 30.1^\circ$, 35.5° , 43.2° , 53.5° , 57.1° , and 62.6° corresponding to the reflection plane indices of (2 2 0), (3 1 1), (4 0 0), (4 2 2), (5 1 1) and (4 4 0) respectively. All the nanoparticles show inverse spinel structure. Likewise, it can be seen that the CS,

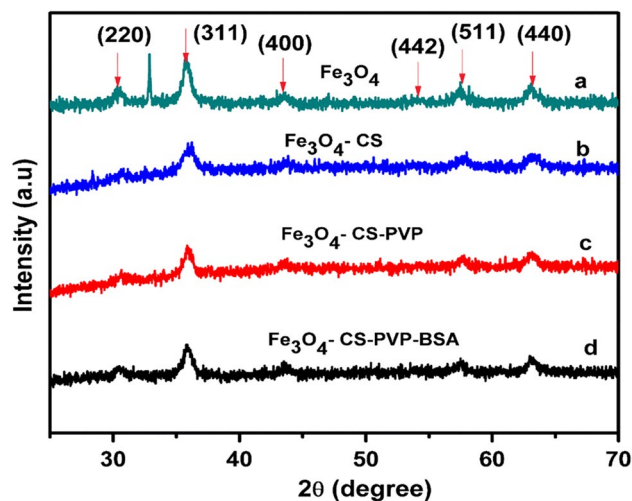


Fig. 2 XRD patterns of a pure Fe_3O_4 , b Fe_3O_4 -CS, c Fe_3O_4 -CS-PVP and d Fe_3O_4 -CS-PVP-BSA nanoparticles

PVP and BSA coating procedure did not result in any phase change of Fe_3O_4 .

Scanning electron microscopy (SEM) analysis

SEM has been working for the surveillance of the surface morphology of the TAM drug-loaded nanocomposites (Fe_3O_4 -CS-TAM, Fe_3O_4 -CS-TAM-PVP and Fe_3O_4 -CS-TAM-PVP-BSA) and is presented in Fig. 3. SEM images of the TAM drug-loaded nanoparticles (Fe_3O_4 -CS-TAM) (Fig. 3a) show that nanoparticles have a generic spherical shape and has smoother surface but with some heterogeneous morphology whereas addition of PVP and BSA to Fe_3O_4 -CS-TAM nanoparticles produces sphere shapes with smoother surface and homogeneous morphology Fig. 3b–d. The outcome of SEM analysis in this study confirms that all the nanoparticles are spherical in shape. Various studies have proved that spherical nanoparticles are the most appropriate for drug delivery applications and have higher possibility for cell passage [50, 51]. Consequently, we report that the TAM-loaded nanocomposites (Fe_3O_4 -CS-TAM, Fe_3O_4 -CS-TAM-PVP and Fe_3O_4 -CS-TAM-PVP-BSA) could be investigated for drug encapsulation efficiency and drug loading.

Atomic force microscopy (AFM) analysis

The surface morphology and size of the prepared nanoparticles were further confirmed by AFM. Figure 4a–c indicates the 2-dimensional (2-D) topographical views of Fe_3O_4 -CS-TAM, Fe_3O_4 -CS-TAM-PVP and Fe_3O_4 -CS-TAM-PVP-BSA nanoparticles and the relating 3-dimensional (3-D) images are displayed in Fig. 4a₁–c₁. Figure 4a–c demonstrates that all the prepared nanoparticles have smooth surface with nearly sphere-shaped morphology. The average diameter of the developed Fe_3O_4 -CS-TAM, Fe_3O_4 -CS-TAM-PVP and Fe_3O_4 -CS-TAM-PVP-BSA nanoparticles shown in Fig. 4a–c is 160.3, 258.9, and 303.7 nm, respectively, and the average height of developed nanoparticles is found to be 29.4, 60.6 and 91.9 nm, respectively, as exhibited in Fig. 4a₁–c₁. The particle size got from AFM is greatly lesser than that of the size got from Zetasizer. As we probably are aware, Zetasizer gives the data of the particles inflated in solution, whereas AFM demonstrates the images of the particles spread and dried on a plain glass plate surface. The height is greatly lesser than the diameter; this can be described by the composition of nanoparticles, which were adaptable polymers that can bring about the collapse of nanoparticles during the observation [52].

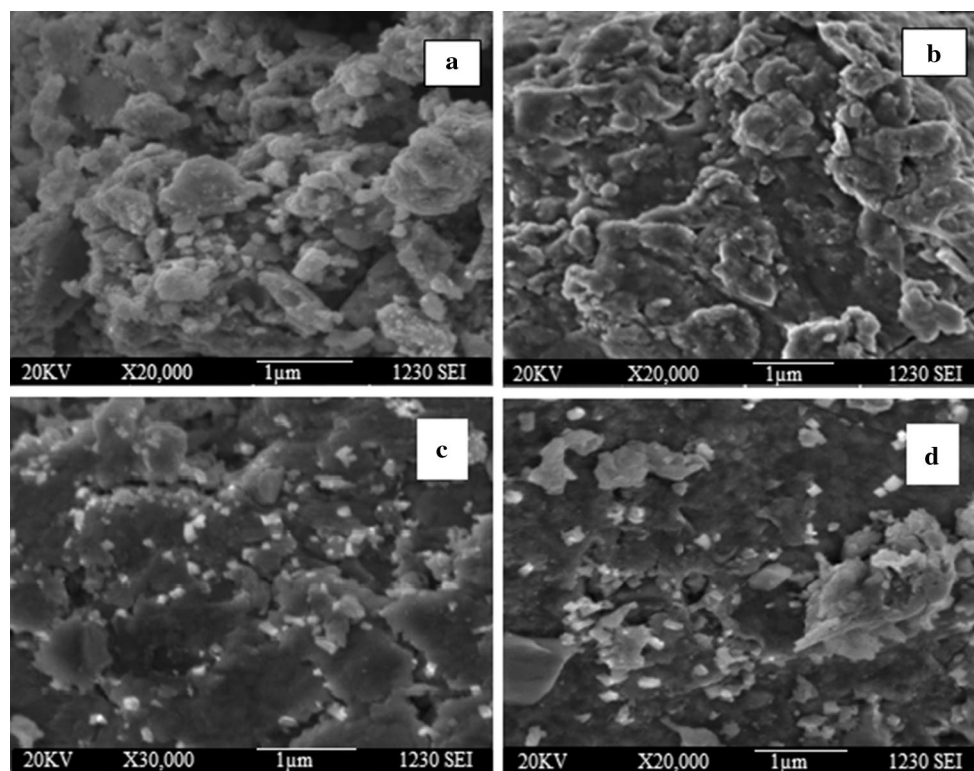


Fig. 3 SEM images of tamoxifen-loaded **a** Fe_3O_4 -CS-TAM, **b** Fe_3O_4 -CS-TAM-PVP and **c, d** Fe_3O_4 -CS-TAM-PVP-BSA nanoparticles

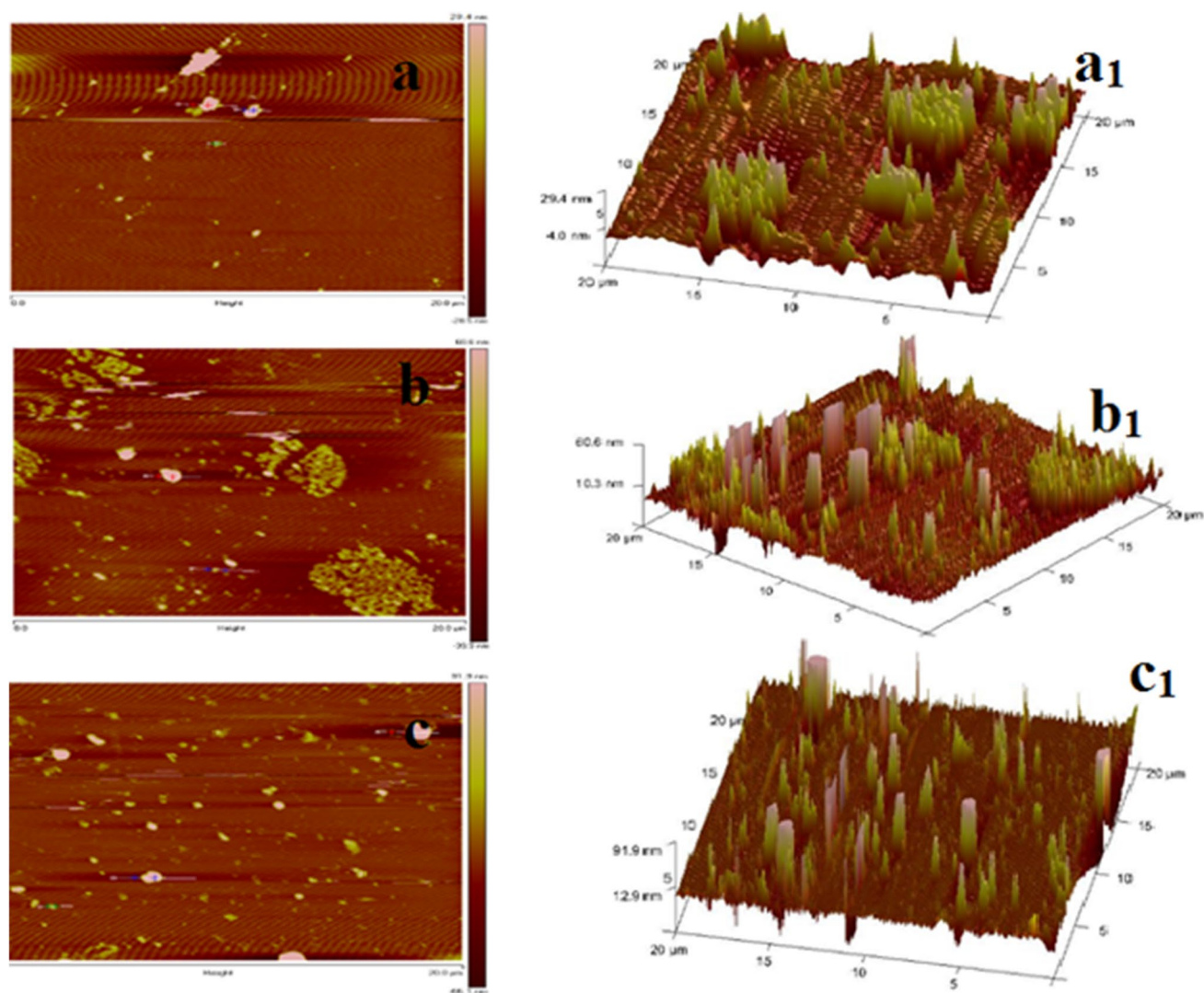


Fig. 4 2D and 3D AFM images of **a, a₁** Fe₃O₄-CS-TAM, **b, b₁** Fe₃O₄-CS-TAM-PVP and **c, c₁** Fe₃O₄-CS-TAM-PVP-BSA nanoparticles

Transmission electron microscopy (TEM) analysis

The surface morphology and size of the raw Fe₃O₄ and tamoxifen drug-loaded Fe₃O₄-CS, Fe₃O₄-CS-PVP and Fe₃O₄-CS-PVP-BSA nanoparticles was observed by TEM as revealed in Fig. 5. Figure 5a shows that the raw Fe₃O₄ nanoparticles were successfully prepared with nanometer size. Fe₃O₄ nanoparticles appear to have a roughly uniform spherical morphology, with an average diameter of 20–50 nm. However, the TEM image shows that the Fe₃O₄ nanoparticles were simply aggregated. It might be due to small sizes, large specific surface area, surface energy and magnetization effect. Figure 5b–d demonstrates the TEM images of drug-loaded Fe₃O₄-CS-TAM, Fe₃O₄-CS-TAM-PVP and Fe₃O₄-CS-TAM-PVP-BSA nanoparticles. Figure 5b indicates that the Fe₃O₄-CS-TAM nanoparticles have a spherical morphology with an average

diameter of 30–50 nm. Besides, addition of PVP and BSA to Fe₃O₄-CS-TAM nanoparticles displays spherical morphology and are homogeneously distributed, with an average diameter ranging from 30–50 nm (Fig. 5c, d), which is clearly evident when compared to Fig. 5b.

Circular dichroism spectroscopy (CD)

The interactions of BSA and Fe₃O₄-CS-TAM-PVP-BSA nanocomposites were examined by circular dichroism spectroscopy (Fig. 6). CD spectra of the samples were measured by monitoring the changes of the signal from 190 to 270 nm. The CD spectra clearly displays that BSA was incorporated into the nanoparticles. Analysis of the CD spectra can provide information about structural changes occurring in the BSA present in nanocomposites. As expected for a protein that is predominately α -helical [53, 54]. The CD spectrum of

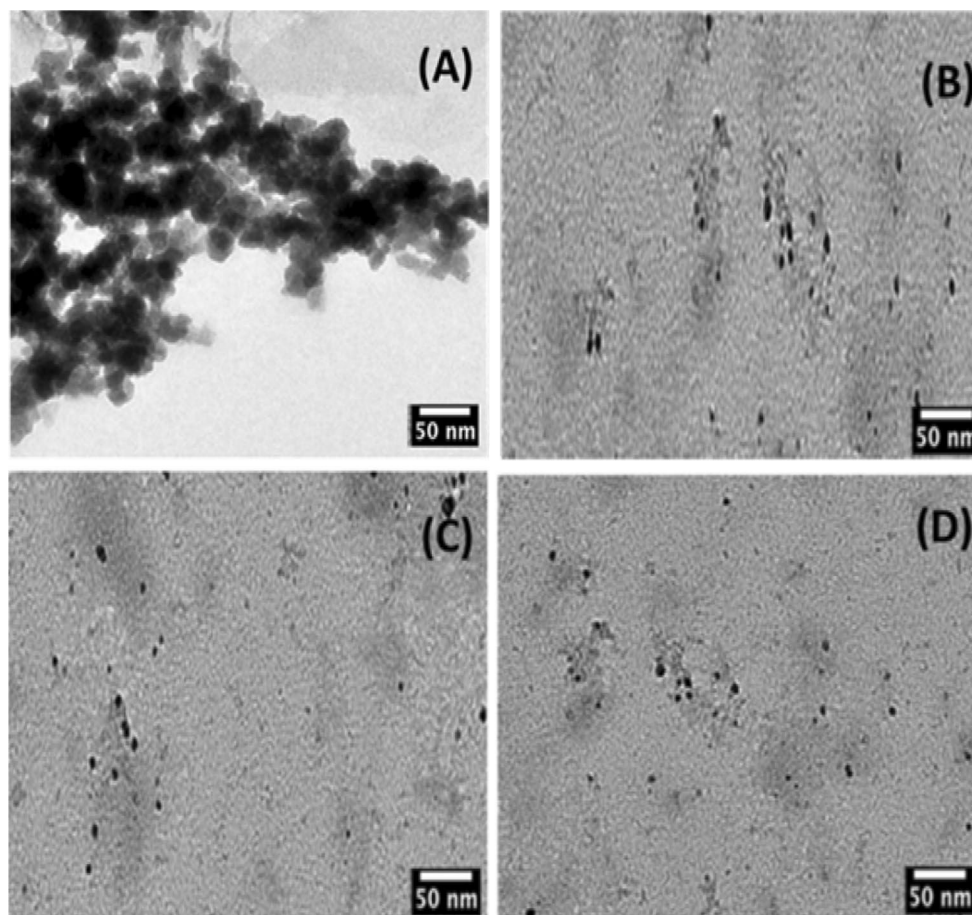


Fig. 5 TEM images of raw Fe_3O_4 (a), and tamoxifen-loaded Fe_3O_4 -CS (b), Fe_3O_4 -CS-PVP (c), Fe_3O_4 -CS-PVP-BSA (d) nanoparticles

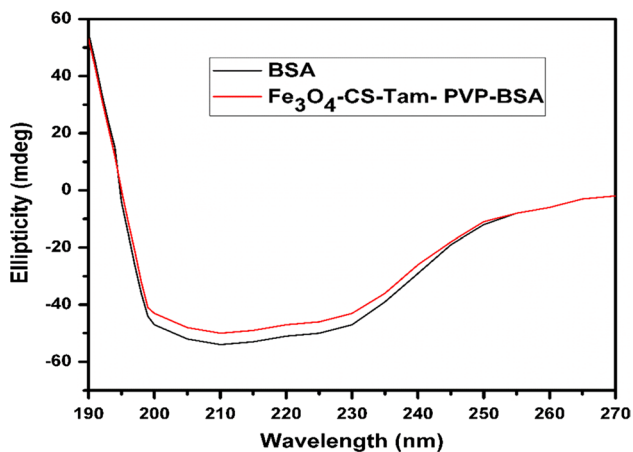


Fig. 6 Circular dichroism spectra of raw BSA and Fe_3O_4 -CS-TAM-PVP-BSA nanoparticles

BSA contains two strong negative bands at 208 and 222 nm that are characteristic of its α -helical content. The intensity of this double minimum reflects the amount of helicity in BSA. Fractional contents of secondary structure in BSA ($f\alpha$,

Table 3 Fractional contents ($f\alpha$, $f\beta$, f turn and f random) of secondary structure for pure BSA solution and Fe_3O_4 -CS-TAM-PVP-BSA nanocomposites

	α -Helix	β -Structure	Turns	Random
BSA	67	6	15	25
Fe_3O_4 -CS-TAM-PVP-BSA	61	8	20	30

$f\beta$, f turn and f random) and Fe_3O_4 -CS-TAM-PVP-BSA are shown in Table 3. When polysaccharides interact with a globular protein, the intermolecular forces responsible for maintaining the secondary and tertiary structures can be altered, resulting in a conformational change in the protein. The addition of BSA into the Fe_3O_4 -CS-TAM-PVP solution leads to a slight decrease in the 222 nm trough and a small increase at 209 nm. The decrease in the content of α -helical structure from 67 to 61% was obtained after applying a curve fitting program.

Magnetic properties

The magnetic properties of pure Fe_3O_4 and Fe_3O_4 -CS, Fe_3O_4 -CS-PVP and Fe_3O_4 -CS-PVP-BSA nanocomposites were measured out at room temperature by vibrating sample magnetometer (VSM), as shown in Fig. 7. The nature of remanence and zero coercivity in all samples (Fe_3O_4 -CS, Fe_3O_4 -CS-PVP and Fe_3O_4 -CS-PVP-BSA) indicate their superparamagnetic behavior. According to Fig. 7, the saturation magnetization values of pure Fe_3O_4 nanoparticles, Fe_3O_4 -CS, Fe_3O_4 -CS-PVP and Fe_3O_4 -CS-PVP-BSA nanocomposites are 67, 42, 38 and 33 emu/g, respectively. The saturation magnetization value of the Fe_3O_4 nanoparticles is slightly greater than that of the Fe_3O_4 -coated CS, PVP and BSA (Fe_3O_4 -CS, Fe_3O_4 -CS-PVP and Fe_3O_4 -CS-PVP-BSA) nanoparticles (i.e., addition of CS, PVP and BSA with Fe_3O_4 nanoparticles leads to the reduction in saturation magnetization values of Fe_3O_4 nanoparticles). This is because of the increased quantity of polymers fused in the polymer-coated magnetite suspension. With a vital part of surface atoms, whichever crystalline issue inside the surface layer can likewise prompt an important decrease in the saturation magnetization of nanoparticles [55].

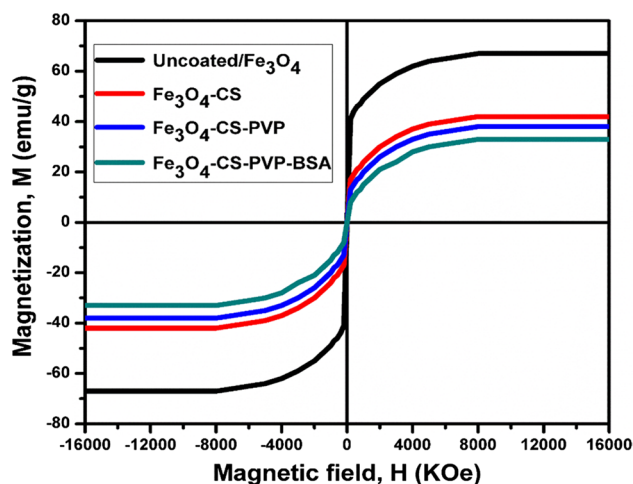


Fig. 7 VSM magnetization curves of Fe_3O_4 Nps and Fe_3O_4 -CS, Fe_3O_4 -CS-PVP and Fe_3O_4 -CS-PVP-BSA nanoparticles

Table 4 Encapsulation efficiency (EE) and loading capacity (LC) of TAM-loaded nanoparticles

Concentration of TAM (%)	Fe_3O_4 -CS-TAM nanoparticles		Fe_3O_4 -CS-TAM-PVP nanoparticles		Fe_3O_4 -CS-TAM-PVP-BSA nanoparticles	
	% of EE	% of LC	% of EE	% of LC	% of EE	% of LC
10	63.60 ± 2.11	41.22 ± 1.10	70.34 ± 2.20	45.12 ± 1.45	79.56 ± 2.34	50.62 ± 1.30
20	68.23 ± 2.49	48.42 ± 1.23	75.04 ± 2.91	53.58 ± 1.72	83.11 ± 2.55	59.36 ± 1.59
30	76.09 ± 2.12	53.23 ± 1.40	79.12 ± 2.21	58.08 ± 1.54	88.83 ± 2.45	65.75 ± 1.54
40	79.25 ± 2.71	60.21 ± 1.52	83.23 ± 2.83	63.43 ± 1.82	90.22 ± 2.17	70.65 ± 1.28
50	82.10 ± 2.01	65.12 ± 1.71	85.18 ± 2.16	68.14 ± 1.56	96.45 ± 2.12	75.38 ± 1.75

Encapsulation efficiency (EE) and loading capacity (LC)

Drug loading and encapsulation efficiency are vital sources for drug delivery systems. In this study, TAM drug was introduced into the drug delivery systems through encapsulation in Fe_3O_4 -CS, Fe_3O_4 -CS-PVP and Fe_3O_4 -CS-PVP-BSA nanocomposites. The EE and LC of Fe_3O_4 -CS-TAM, Fe_3O_4 -CS-TAM-PVP and Fe_3O_4 -CS-TAM-PVP-BSA nanocomposites were evaluated by UV spectrophotometry. The EE and LC of the systems are found to be 82.10 ± 2.01 , 85.18 ± 2.16 and 96.45 ± 2.12 and 65.12 ± 1.71 , 68.14 ± 1.56 and $75.38 \pm 1.75\%$, respectively, for the (50%) TAM-loaded (Fe_3O_4 -CS-TAM, Fe_3O_4 -CS-TAM-PVP and Fe_3O_4 -CS-TAM-PVP-BSA) nanocomposites as depicted in Table 4. The initial concentration of TAM assumed a significant part in deciding the drug EE and drug LC of the Fe_3O_4 -CS, Fe_3O_4 -CS-PVP and Fe_3O_4 -CS-PVP-BSA nanocomposites systems (Table 4). At the point when the concentration of TAM is increased, the EE and LC of Fe_3O_4 -CS, Fe_3O_4 -CS-PVP and Fe_3O_4 -CS-PVP-BSA nanocomposites systems also increased. The EE & LC of Fe_3O_4 -CS-PVP-BSA nanocomposites are, to some degree, more prominent than those of the Fe_3O_4 -CS and Fe_3O_4 -CS-PVP nanocomposites when the initial concentration of TAM is same, which may be attributed to the fact that Fe_3O_4 -CS-PVP-BSA nanocomposites have more electrostatic interaction than Fe_3O_4 -CS, and Fe_3O_4 -CS-PVP nanocomposites with TAM. This demonstrates that the Fe_3O_4 -CS-PVP-BSA nanocomposites system is undeniably a favorable contender for drug carrier materials.

Swelling studies

The swelling nature of any polymer network depends upon the nature of the polymer, degree of cross-linking and polymer solvent compatibility. Nevertheless, in the case of ionic networks, swelling nature is based on mass transfer limitations, ionic interaction and ion exchange [56].

Swelling properties of Fe_3O_4 -CS-PVP-BSA nanocomposites is of great prominence for medical applications and were observed and are displayed in Fig. 8 after 1 day of incubation in the PBS solution (pH 4.0). Figure 8

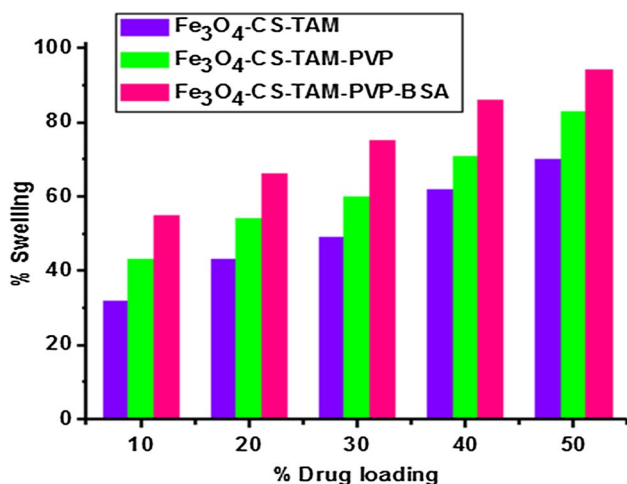


Fig. 8 Percentage swelling degree of the Fe₃O₄-CS, Fe₃O₄-CS-PVP and Fe₃O₄-CS-PVP-BSA nanoparticles with different percentage (%) drug loadings

indicates the percentage (%) of swelling for the Fe₃O₄-CS, Fe₃O₄-CS-PVP and Fe₃O₄-CS-PVP-BSA nanocomposites combined with different (10, 20, 30, 40, 50%) drug loadings (pH 4.0) at 37 °C. Figure 8 shows that the percentage of swelling of the nanocomposites increased gradually after the addition of PVP and BSA with TAM drug-loaded

nanocomposites (Fe₃O₄-CS-TAM). This shows that the percentage (%) swelling increases with increase in drug loading in the Fe₃O₄-CS, Fe₃O₄-CS-PVP and Fe₃O₄-CS-PVP-BSA nanocomposites.

In vitro drug release studies

Figure 9 represents the in vitro drug release profile of Tamoxifen (TAM) from Fe₃O₄-CS-TAM, Fe₃O₄-CS-TAM-PVP and Fe₃O₄-CS-TAM-PVP-BSA nanocomposites at two different pH values (pH 4.0 and 7.4) and two different temperatures (37 and 45 °C). The addition of PVP and BSA increases the hydrophilic and biocompatible nature of the nanoparticles. Far along, increase in drug release time is seen after the adding, because of the reality, reduction in polymer matrix prompts to decrease the free space for the movement of solute through the polymer matrix. The release of TAM from the (Fe₃O₄-CS-TAM, Fe₃O₄-CS-TAM-PVP and Fe₃O₄-CS-TAM-PVP-BSA) nanocomposites are dependent on the pH value of the PBS medium (4.0 and 7.4) and two temperatures—physiological temperature (37 °C) and low hyperthermal temperature (45 °C). The dependence of TAM release from the drug carrier under these conditions is presented in Fig. 9.

Drug release (TAM) is slow and sustainable under neutral environment (pH 7.4). However, TAM release is significantly

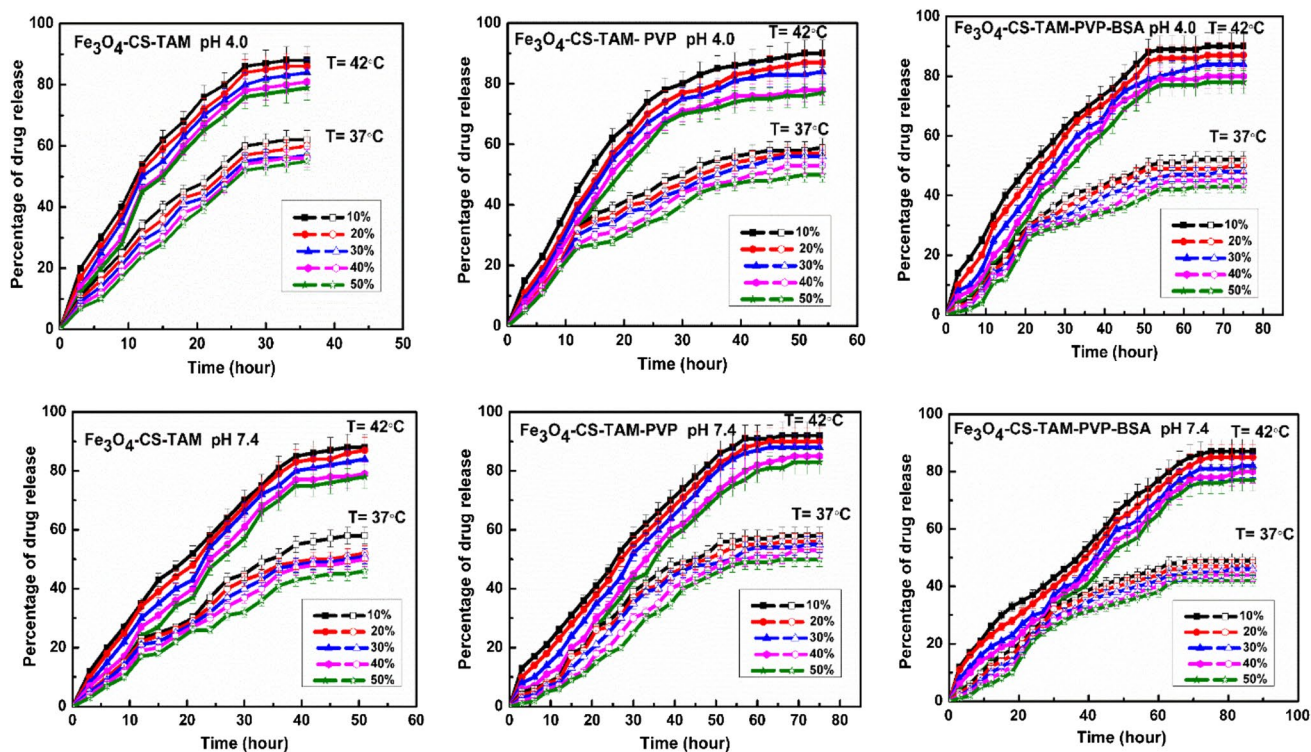


Fig. 9 In vitro drug release analysis of tamoxifen-encapsulated (Fe₃O₄-CS-TAM, Fe₃O₄-CS-TAM-PVP and Fe₃O₄-CS-TAM-PVP-BSA) nanoparticles at neutral condition (pH 7.4) and acidic conditions (pH 4.0) at 37 and 42 °C. Each point represents the Mean ± SD

faster under acidic environment (pH 4.0). The improved drug release in the acidic pH can be possible only due to the protonation of the drug happened at lower pH value (pH 4.0), which released chemisorbed drug molecules into the medium. Likewise, surface charges of free amino groups of CS NPs became positive at lower pH (acidic environment pH 4.0), the electrostatic interaction of drug and amino group of CS NPs is reduced and the drug release process is enabled. These outcomes display the pH-activated drug release characteristic feature from the new drug release system and this is of specific importance. It can be understood that most part of the drug remains in the carrier for a significant time period at pH 7.4. This is a clear sign of the potential for an extended drug maintenance time in blood flow and henceforth it leads to the reduction of the side effects to the normal tissues. As well, when the drug-loaded nanocomposites are taken up by tumor cells through endocytotic process, there are chances for a rapider release at lower pH, i.e., around the tumor site or inside the endosome and lysosome of tumor cells. This leads to an important progress in cancer treatment efficiency [57]. Nevertheless, at 37 °C, the release of TAM from Fe₃O₄-CS-TAM, Fe₃O₄-CS-TAM-PVP and Fe₃O₄-CS-TAM-PVP-BSA nanocomposites is less than at 45 °C for both test pHs of 4.0 and 7.4. The outcomes in Fig. 9. unmistakably demonstrate that on increasing temperature, the drug release increases.

The noticed increase in drug release at higher temperature may be accredited to the fact that, on increasing temperature the H-bonds between the drug molecules and the network chains are cracked, consequently altering bound water into free water. As indicated by the release data, fast and more prominent release rates are displayed in the larger quantity of drug (50%) than the smaller quantity of drug (10%). When smaller quantity of drug was loaded into the

nanocomposites, the release rate is slower due to the extra free void spaces, through which a slight number of drug molecules could conveyance. For magnetic targeting drug delivery system, the grouping of chemotherapy with hyperthermia (42–45 °C) is easy to comprehend when an exterior restricted substituting magnetic field is included. According to the outcomes, Fe₃O₄-CS-TAM-PVP-BSA nanocomposites system is sufficiently proficient to be a good magnetic targeting carrier with a double therapeutic impact for the treatment of tumor cells.

Cytotoxicity studies

To examine whether the created nanoparticles could be utilized for delivering drugs, for example, TAM to VERO and MCF-7 cell lines, a relative cytotoxicity study on the impacts of free TAM, TAM-loaded nanocomposites (Fe₃O₄-CS-TAM, Fe₃O₄-CS-TAM-PVP and Fe₃O₄-CS-TAM-PVP-BSA) and unloaded Fe₃O₄-CS-PVP-BSA nanocomposites was done. The cells were exposed to different concentrations of free TAM, TAM-loaded nanocomposites (Fe₃O₄-CS-TAM, Fe₃O₄-CS-TAM-PVP and Fe₃O₄-CS-TAM-PVP-BSA) and unloaded (Fe₃O₄-CS-PVP-BSA) nanocomposites and incubated for 48 h and the results are given in Fig. 10. TAM-loaded nanocomposites (Fe₃O₄-CS-TAM, Fe₃O₄-CS-TAM-PVP and Fe₃O₄-CS-TAM-PVP-BSA) showed a marginally higher cytotoxicity than that of free TAM at the concentrations ranging from 5–75 µg/mL in MCF-7 cells, while unloaded Fe₃O₄-CS-PVP-BSA nanocomposites revealed less toxicity for both MCF-7 and VERO cells. These outcomes plainly show that TAM-loaded (Fe₃O₄-CS-TAM-PVP-BSA) nanocomposites could actuate cytotoxic answer to MCF-7 cell

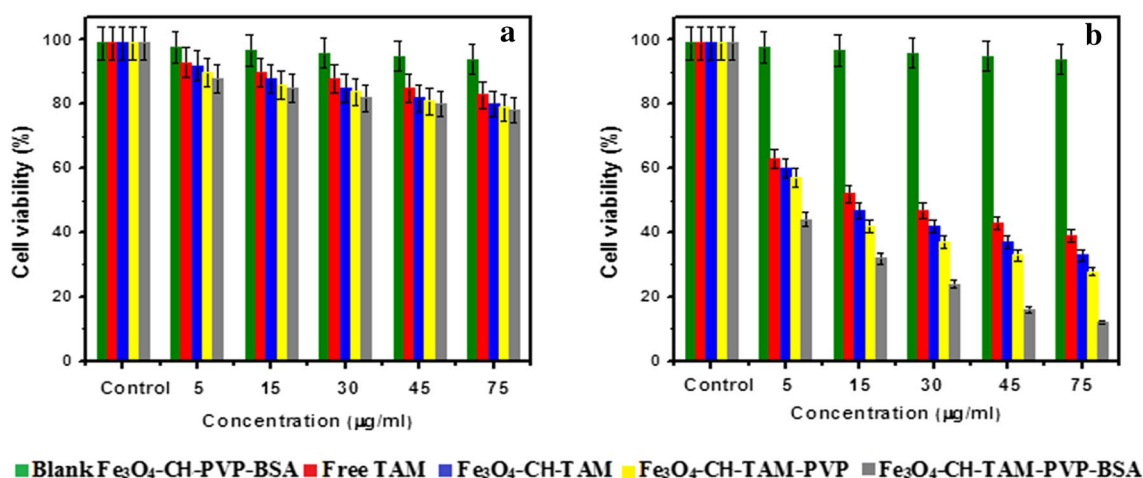


Fig. 10 Cell viability of free TAM, TAM loaded (Fe₃O₄-CS-TAM, Fe₃O₄-CS-TAM-PVP and Fe₃O₄-CS-TAM-PVP-BSA) and unloaded (Fe₃O₄-CS-PVP-BSA) magnetic polymer composite nanoparticles **a** VERO cells and **b** MCF-7 cells treated with TAM

lines to a more prominent score than TAM-loaded ($\text{Fe}_3\text{O}_4\text{-CS-TAM}$, $\text{Fe}_3\text{O}_4\text{-CS-TAM-PVP}$) nanocomposites. As the cell viability is concentration-dependent, increase in the concentrations led to a diminishing in cell viability as exemplified in Fig. 10. However, 80% of the cells are viable indicating the non-toxicity of free TAM, TAM-loaded nanocomposites ($\text{Fe}_3\text{O}_4\text{-CS-TAM}$, $\text{Fe}_3\text{O}_4\text{-CS-TAM-PVP}$ and $\text{Fe}_3\text{O}_4\text{-CS-TAM-PVP-BSA}$) and unloaded $\text{Fe}_3\text{O}_4\text{-CS-PVP-BSA}$ nanocomposites toward VERO cells. According to the results, the unloaded $\text{Fe}_3\text{O}_4\text{-CS-PVP-BSA}$ nanocomposites did not show any obvious cytotoxicity at the concentration ranging from 5–75 $\mu\text{g/mL}$ and show good biocompatibility, and TAM-loaded ($\text{Fe}_3\text{O}_4\text{-CS-TAM-PVP-BSA}$) composites have higher cytotoxicity.

Apoptosis analysis by flow cytometry

The apoptotic profile of free tamoxifen, drug-loaded ($\text{Fe}_3\text{O}_4\text{-CS-TAM}$, $\text{Fe}_3\text{O}_4\text{-CS-TAM-PVP}$ and $\text{Fe}_3\text{O}_4\text{-CS-TAM-PVP-BSA}$) nanoparticles and unloaded ($\text{Fe}_3\text{O}_4\text{-CS-TAM-PVP-BSA}$) nanoparticles on MCF-7 cell line was evaluated using flow cytometry after 48 h of exposure. The apoptosis inducing efficiency on MCF-7 cell line was investigated. Data from flow cytometry (Fig. 11) showed that TAM drug-loaded $\text{Fe}_3\text{O}_4\text{-CS-TAM}$, $\text{Fe}_3\text{O}_4\text{-CS-TAM-PVP}$ and $\text{Fe}_3\text{O}_4\text{-CS-TAM-PVP-BSA}$ nanoparticles had significantly higher apoptotic activity than free tamoxifen and unloaded $\text{Fe}_3\text{O}_4\text{-CS-TAM-PVP-BSA}$ nanoparticles. The improved apoptotic activity of $\text{Fe}_3\text{O}_4\text{-CS-TAM-PVP-BSA}$ nanoparticles could be due to the better uptake and greater accumulation of nanoparticulate TAM inside the tumor cells [58]. With an increase in the concentration of nanoparticles, number of apoptotic cells were increased suggesting

that nanoparticles could induce cell apoptosis as shown in Fig. 11.

Conclusions

We have exhibited a basic and successful method to synthesize $\text{Fe}_3\text{O}_4\text{-CS}$, $\text{Fe}_3\text{O}_4\text{-CS-PVP}$ and $\text{Fe}_3\text{O}_4\text{-CS-PVP-BSA}$ nanocomposites, and these nanocomposites can go about as a potential drug delivery carrier in solution. SEM, AFM and TEM images displayed that the particles are monodispersed and have spherical-shaped structure. As evidenced from FTIR, there is good interaction between drug and prepared nanocomposites functional groups. XRD analysis proved the inverse spinel structure of the Fe_3O_4 nanoparticles. The results of VSM exhibited that the prepared nanocomposites have a superparamagnetic behavior. Swelling studies indicates that the percentage of swelling rises with rise in the percentage of drug loading. The MTT assay showed that unloaded ($\text{Fe}_3\text{O}_4\text{-CS-PVP-BSA}$) nanocomposites are non-toxic to VERO and MCF-7 cell lines, whereas the TAM-loaded ($\text{Fe}_3\text{O}_4\text{-CS-TAM-PVP-BSA}$) nanocomposites presented an exact toxicity to MCF-7 cell lines. Overall, these findings suggest that $\text{Fe}_3\text{O}_4\text{-CS-PVP-BSA}$ nanocomposites could be used as a best carrier to deliver anticancer drugs like TAM with an improved therapeutic activity of TAM.

Acknowledgements One of the authors G. Prabha would like to acknowledge the Department of Science and Technology (DST) under the Science and Engineering Research Board (SERB) for the award of her National Post-Doctoral fellowship (PDF/2016/002403). Authors also thank Centralised Instrumentation Laboratory, Tamil Nadu Veterinary and Animal Sciences University, India, and C. Ramkumar Research scholar, Department of Metallurgical and Materials Engineering, NIT Rourkela for providing technical support and necessary facilities.

References

1. T.K. Jain, M.A. Morales, S.K. Sahoo, D.L. Leslie-Pelecky, V. Labhasetwar, *Mol. Pharm.* **2**, 194–205 (2005)
2. I. Hilger, K. Fruhauf, W. Abdra, R. Hiergeist, R. Hergt, W.A. Kaiser, *Acad. Radiol.* **9**, 198–202 (2002)
3. M. Zhao, M.F. Kircher, L. Josephson, R. Weissledre, *Bioconjug. Chem.* **13**, 840–844 (2002)
4. J.W.M. Bulte, T. Douglas, B. Witwer, S.-C. Zhang, E. Strable, B.K. Lewis, H. Zywicke, B. Miller, P.V. Gelderen, B.M. Moskowitz, I.D. Duncan, J.A. Frank, *Nat. Biotechnol.* **19**, 1141–1147 (2001)
5. J.P. Butler, S.M. Kelly, *Biorheology* **35**, 193–209 (1998)
6. D. Dressman, H. Yan, G. Traverso, K.W. Kinzler, B. Vogelstein, *Proc. Natl. Acad. Sci.* **100**, 8817–8822 (2003)
7. R.E. Zigeuner, R. Riesenber, H. Pohla, A. Hofstetter, R. Oberneder, *J. Urol.* **169**, 701–705 (2003)
8. R. De Palma, J. Trekker, S. Peeters, M.J. Van Bael, K. Bonroy, R. Wirix-Speetjens, G. Reekmans, W. Laureyn, G. Borghs, G. Maes, *J. Nanosci. Nanotechnol.* **7**, 4626–4641 (2007)

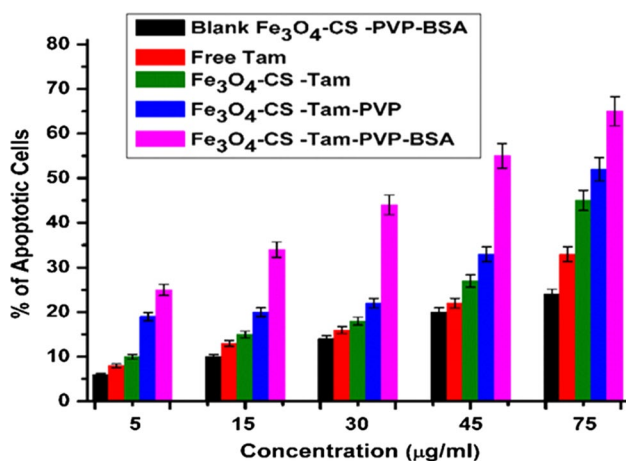


Fig. 11 % of Apoptotic cells analyzed by flow cytometry

9. T. Gordon, B. Perlstein, O. Houbara, I. Felner, E. Banin, S. Margel, *Colloids Surf. A Physicochem. Eng. Asp.* **374**, 1–8 (2011)
10. J. Jayapaul, M. Hodenius, S. Arns, W. Lederle, T. Lammers, P. Comba, F. Kiessling, J. Gaetjens, *Biomaterials* **32**, 5863–5871 (2011)
11. F. Jiang, Y. Fu, Y. Zhu, Z. Tang, P. Sheng, *J. Alloys Compd.* **543**, 43–48 (2012)
12. S.L. Easo, P.V. Mohanan, *Carbohydr. Polym.* **92**, 726–732 (2013)
13. A.J. Cole, A.E. David, J. Wang, C.J. Galban, H.L. Hill, V.C. Yang, *Biomaterials* **32**, 2183–2193 (2011)
14. C. Schweiger, C. Pietzonka, J. Heverhagen, T. Kissel, *Int. J. Pharm.* **408**, 130–137 (2011)
15. A.K. Gupta, M. Gupta, *Biomaterials* **26**, 1565–1573 (2005)
16. C.C. Berry, S. Wells, S. Charles, G. Aitchison, A.S.G. Curtis, *Biomaterials* **25**, 5405–5413 (2004)
17. D.K. Kim, M. Mikhaylova, F.H. Wang, J. Kehr, B. Bjelke, Y. Zhang, T. Tsakalagos, M. Muhammed, *Chem. Mater.* **15**, 4343–4351 (2003)
18. M. Mikhaylova, D.K. Kim, C.C. Berry, A. Zagorodni, M. Toprak, A.S.G. Curtis, M. Muhammed, *Chem. Mater.* **16**, 2344–2354 (2004)
19. L.A. Harris, J.D. Goff, A.Y. Carmichael, J.S. Riffle, J.J. Harburn, T.G. St. Pierre, M. Saunders, *Chem. Mater.* **15**, 1367–1377 (2003)
20. S. Wan, J. Huang, H. Yan, K. Liu, *J. Mater. Chem.* **16**, 298–303 (2006)
21. M.N. Kumar, R.A. Muzzarelli, C. Muzzarelli, H. Sashiwa, A.J. Domb, *Chem. Rev.* **104**, 6017–6084 (2004)
22. J. Huang, L.H. Bu, J. Xie, K. Chen, Z. Cheng, X.G. Li, X.Y. Chen, *ACS Nano* **4**, 7151–7160 (2010)
23. N. Arsalani, H. Fattahi, M. Nazarpour, *Express Polym. Lett.* **4**, 329–338 (2010)
24. Z.M. Zhou, A.C. Anselmo, S. Mitragotri, *Adv. Mater.* **25**, 2723–2727 (2013)
25. N.F. Rodrigues, E.T. Bernardes, R.P. Rocha, *Vaccine* **31**, 5062–5066 (2013)
26. A.O. Elzoghby, W.M. Samy, N.A. Elgindy, *J. Control. Release* **157**, 168–182 (2012)
27. B. Elsadek, F. Kratz, *J. Control. Release* **157**, 4–28 (2012)
28. J. McGregor, V. Jorda, *Pharmacol. Rev.* **50**, 151–196 (1998)
29. D.K. Wyld, J.D. Chester, T.J. Perren, *Endocr. Relat. Cancer* **5**, 97–110 (1998)
30. V.C. Jordan, *Breast Cancer Res. Treat.* **31**, 41–52 (1994)
31. S. Mandlekar, A.N. Kong, *Apoptosis* **6**, 469–477 (2001)
32. P.N. Munster, C.A. Hudis, *Hematol. Oncol. Clin. North Am.* **13**, 391–413 (1999)
33. C. Cuvier, L. Roblot treupel, J.M. Millot, G. Lizard, S. Chevillard, M. Manfait, P. Couvreur, M.F. Poupon, *Biochem. Pharmacol.* **44**, 509–517 (1992)
34. J. Park, P.M. Fong, J. Lu, K.S. Russell, C.J. Booth, W.M. Saltzman, T.M. Fahmy, *Nanomed. Nanotechnol. Biol. Med.* **5**, 410–418 (2009)
35. E. Gulyaev, S.E. Gelperina, I.N. Skidan, A.S. Antropov, G.Y. Kivman, J. Kreuter, *Pharm. Res.* **16**, 1564–1569 (1999)
36. K.A. Janes, M.P. Fresneau, A. Marazuela, A. Fabra, M.J. Alonso, *J. Control. Release* **73**, 255–267 (2001)
37. N. Lukyanov, T.A. Elbayoumi, A.R. Chakilam, V.P. Torchilin, *J. Control. Release* **100**, 135–144 (2004)
38. E. Leo, M.A. Vandelli, R. Camerini, F. Forni, *Int. J. Pharm.* **155**, 75–82 (1997)
39. S. Dreis, F. Rothweiler, M. Michaelis, J. Cinatl, J. Kreuter, K. Langer, *Int. J. Pharm.* **341**, 207–214 (2007)
40. G. Prabha, V. Raj, *Biomed. Pharmacother.* **80**, 173–182 (2016)
41. P. Li, Y. Wang, Z. Peng, F. She, L. Kong, *Carbohydr. Polym.* **85**, 698–704 (2011)
42. M. Rajan, V. Raj, A.A. Al-Arfaj, A.M. Murugan, *Int. J. Pharm.* **453**, 514–522 (2013)
43. S. Papadimitriou, D. Bikiaris, K. Avgoustakis, E. Karavas, M. Georgarakis, *Carbohydr. Polym.* **73**, 44–54 (2008)
44. N. Devi, T.K. Maji, *Drug Dev. Ind. Pharm.* **36**, 56–63 (2010)
45. B. Wilson, M.K. Samanta, M.S. Muthu, G. Vinothapooshan, *Ther. Deliv.* **2**, 599–609 (2011)
46. F.A. Oyarzun-Ampuero, J. Brea, M.I. Loza, D. Torres, M.J. Alonso, *Int. J. Pharm.* **381**, 122–129 (2009)
47. J. Jingou, H. Shilei, L. Weiqi, W. Danjun, W. Tengfei, X. Yi, *Colloids Surf. B* **83**, 103–107 (2011)
48. J. Schillers, L. Naji, R. Trampel, W. Ngwa, R. Knauss, K. Arnold, in *Osteoarthritis: Methods and Protocols*, ed. by F. De Ceuninck, P. Pastoureaux, M. Sabatini (Humana Press, Totowa, 2004), pp. 287–302
49. P. Nanta, W. Sakolpap, K. Kasemwong, (ICCES'2012), Bangkok, (2012)
50. S. Venkatraman, J.L. Hedrick, Z.Y. Ong, C. Yang, *Adv. Drug Deliv. Rev.* **63**, 1228–1246 (2011)
51. X.Q. Zhang, X. Xua, N. Bertrand, E. Pridgenb, A. Swamia, O.C. Farokhzad, *Adv. Drug Deliv. Rev.* **64**, 1363–1384 (2012)
52. S.C. Neves, L.S. Moreira Teixeira, L. Moroni, R.L. Reis, C.A. Van Blitterswijk, N.M. Alves, M. Karperien, J.F. Mano, *Biomaterials* **32**, 1068–1079 (2011)
53. G. Holzwarth, P. Doty, *J. Am. Chem. Soc.* **87**, 218–228 (1965)
54. N.S. Quiming, R.B. Vergel, M.G. Nicolas, J.A. Villanueva, *J. Health Sci.* **51**, 8–15 (2005)
55. H. Cao, J. He, L. Deng, X. Gao, *Appl. Surf. Sci.* **255**, 7974–7980 (2009)
56. S. Frank, P.C. Lauterbur, *Nature* **363**, 334–336 (1993)
57. H. Zhang, C. Wang, B. Chen, X. Wang, C.B. Chen, *Int. J. Nanomed.* **7**, 235–242 (2012)
58. C. Mohanty, S.K. Sahoo, *Biomaterials* **31**, 6597–6611 (2010)